Research Square

Preprints are preliminary reports that have not undergone peer review.
They should not be considered conclusive, used to inform clinical practice,
or referenced by the media as validated information.

Three-dimensional finite element analysis of the effects of MARPE and RME on the expansion of the arches of craniomandibular complexes with different degrees of suture fusion

Ye-Ya Yuan

Hao-Peng Wu

School and Hospital of Stomatology, China Medical University, Liaoning Provincial Key Laboratory of Oral Diseases

Bing Liu

Shenyang Stomatological Hospital

Ning-Ning Wang

Shenyang Stomatological Hospital

Yue-Mei Sun

Shenyang Stomatological Hospital

Jie-Yu Yang

The Second Hospital of Shijiazhuang

Xin Li

Hao-Qing Zhang

School and Hospital of Stomatology, Tianjin Medical University

JiHui Liu

liujihui126@126.com

Shenyang Children's Hospital

Research Article

Keywords:

Posted Date: March 8th, 2026

DOI: https://doi.org/10.21203/rs.3.rs-8422989/v1

License: This work is licensed under a Creative Commons Attribution 4.0 International License.
Read Full License

Additional Declarations: No competing interests reported.

Abstract

Objective

To analyze the stress distribution and displacement trends after on craniomandibular complexes with different degrees of bone seam fusion MARPE and RME for arch expansion using three-dimensional finite element analysis to provide biomechanical guidance for future clinical applications of MARPE.

Methods

A 26-year-old adult female patient with transverse maxillary hypoplasia underwent CBCT, and a 3D finite element model of the craniomandibular complex with unfused and partially fused sutures and two different arch expansion techniques, MARPE and RME, was constructed by setting the material parameters. Four groups of models were created according to the experimental design: Model A was of MARPE with an unfused bone suture; Model B was of MARPE with a partially fused bone suture; Model C was of RME with an unfused bone suture; and Model D was of RME with a partially fused bone suture. Ansys Workbench 2019 software was used to design a transverse forced displacement of 0.25 mm for the model with reference to the clinical arch expander load once and to analyze the stress distribution and displacement of the craniofacial bone, teeth and periodontal tissues under these loading conditions.

Results

The stress distributions on the left and right midpalatal sutures were not completely symmetrical in all the models, and the midpalatal suture was subjected to greater stresses and displacements during MARPE than during RME. The midpalatal suture was closer to a parallel flare with the anterior part slightly larger than the posterior part after MARPE, and the midpalatal suture in Model A was subjected to greater stresses and displacements than Model B was. RME led to a wedge-shaped flare with a large anterior and small posterior area, and the stresses on and displacements of the midpalatal suture in Model C were greater than those in Model D. The jaws were largely displaced laterally in Models A, B, and C and minimally displaced in Model D. The sagittal displacements of the four models tended to be posterior, with outward and backward displacements. The maximum periodontal hydrostatic stresses in all four models were greater than − 0.0047 MPa for all teeth except the abutment teeth and greater than − 0.0047 MPa for the first molar in Model A, whereas the first molar in Model B and the first premolar and first molar in Models C and D were all less than − 0.0047 MPa. The magnitude of the periodontal hydrostatic pressure of the first molar was as follows: Model D > Model C > Model B > Model A. The magnitude of hydrostatic pressure of the periodontium of the first premolar was as follows: Model D > Model C > Model B > Model A.

Conclusions

MARPE led to greater lateral displacement of the jaws and teeth, and the midpalatal suture was closer to parallel expansion with asymmetric stresses on the left and right sides. The stresses on the craniofacial skeleton and lateral displacement of the midpalatal suture, jaws and teeth are greater after MARPE than after RME, suggesting that MARPE is more appropriate for late adolescents and young adults with underdeveloped transverse maxillary structures who have highly fused bone sutures.

1. Introduction

Maxillary transverse deficiency (MTD) is a common malocclusion characterized by a mismatch in the width of the upper and lower dental arches and the underlying bone. This condition may present as unilateral or bilateral crossbite in the posterior teeth area, commonly accompanied by anterior crowding, excessive buccal corridor spaces during smiling, and a high-arched palate[1, 2]. The prevalence of MTD is 8% in patients with primary dentition, 21% in those with mixed dentition, and less than 10% in adults[3–5]. MTD not only affects aesthetic appearance but also impacts functionality, leading to masticatory dysfunction and poor occlusal function, and may even influence nasal development, causing nasal airway constriction, which could contribute to obstructive sleep apnea syndrome[6]. Consequently, issues related to the transverse dimensions associated with MTD as well as its diagnosis and treatment have become the focus of attention among clinicians and scholars.

Currently, various types of palatal expanders are used in clinical settings to treat MTD, including Rapid Maxillary Expansion (RME), Surgically Assisted Rapid Maxillary Expansion (SARME), and Mini Screw-Assisted Maxillary Palatal Expansion (MARPE). RME involves the application of forces along the upper teeth and alveolar ridge to the palatal vault, causing separation of the midpalatal suture and thus increasing the width of the maxilla[7]. As patients age, substantial expansion of the bony arch through the application of orthopedic force during RME in adult MTD patients becomes increasingly challenging. This difficulty arises from the inherent complexity of opening the midpalatal suture, and RME can lead to uncontrollable side effects such as expansion failure, alveolar bone fractures, tooth tilting, root resorption, a reduction in the buccal cortical bone thickness, pain, swelling, and gingival recession[8, 9]. To minimize these side effects, SARME is used in clinical settings to overcome the increased resistance to expansion in young adult patients with MTD due to increased fusion of the midpalatal and posterior maxillary sutures[10]. Although SARME can effectively address the issue of insufficient width development in young adults with high degrees of suture fusion, it still requires general anesthesia, may cause damage to the palatal artery or cranial nerves, is costly and difficult to perform, and is associated with a risk of recurrence [11, 12]. As a nonsurgical alternative for treating MTD patients with high suture fusion, Lee [13]et al. proposed MARPE. MARPE involves the transmission of orthopedic forces generated by expansion directly to the palatal bone through mini screws, overcoming more resistance at the posterior maxilla and achieving more bone-based expansion[8, 14–16].

Furthermore, the efficacy of maxillary expansion is contingent not only on the midpalatal suture but also on the influence of the surrounding tissues and structures of the maxilla. Researchers have determined

that the midpalatal suture region experiences elevated levels of stress following MARPE. Additionally, other bones within the craniofacial skeleton exhibit stress distribution, with the pterygoid, zygomatic, frontal, and nasal bones being particularly affected. Concurrently, periorbital tissues undergo stress concentration[5], and the bony sutures surrounding the maxilla demonstrate stress distribution [17]. It has been demonstrated that the width of the bone suture surrounding the maxilla undergoes augmentation subsequent to MARPE for bow expansion[18]. Consequently, it can be concluded that MARPE not only opens the midpalatal suture but also produces certain forces on the perimandibular structures, thereby resulting in enhanced bony bow expansion. In recent years, MARPE has been widely used in late adolescents and young adults with MTD, as it reduces the risk of surgery-related complications and increases the success rate of expansion[17].

From a biomechanical perspective, the analysis of stress, strain, and displacement in craniomaxillofacial tissue structures following MARPE will facilitate a more comprehensive understanding of the response of these structures to the spreading process. A plethora of research methodologies, including laser holography, strain gauges, and photoelasticity techniques, have been employed to estimate the stress distribution within tissues[19, 20]. However, these methods are inadequate for accurately quantifying the stresses within tissue structures. Three-dimensional finite element analysis (FEA) is a research method that effectively analyzes the stress distribution and predicts the displacement of each tissue structure after MARPE for arch expansion without causing any damage to the tissues. The use of FEA for stress and strain simulation is beneficial for improving the efficacy of MARPE[17, 21]. Three-dimensional finite element analysis (3D FEA) is a noninvasive method that allows virtual simulation of clinical scenarios and evaluation of displacement and stress distribution patterns across different clinical plans. It serves as an effective tool for analyzing the mechanical principles of mini screw-assisted maxillary palatal expansion (MARPE) and determining the stress distribution, displacement, and biomechanical impacts on the surrounding maxillary tissues[5, 22, 23].

However, few 3D finite element studies on MARPE exist, especially analyses that explore the mechanical characteristics of MARPE under varying degrees of suture fusion. Therefore, 3D finite element analysis was performed in this study to evaluate the effectiveness of MARPE by examining the stress distribution and displacement trends in various tissue structures after expansion under different degrees of suture fusion, thereby providing guidance for clinical applications.

2. Materials and methods

2.1 Acquisition of Cone beam CT (CBCT) Data:

Patients are positioned in a seated posture, maintaining a natural head position where the orbital–aural plane is parallel to the ground. During the CBCT scan, patients are instructed to bite gently in a central occlusal position. The scanning range of CBCT encompasses the region from the brow ridge to the base

of the chin, capturing a total of 528 scan images with a slice thickness of 0.25 mm, thereby enabling the acquisition of comprehensive CBCT data.

2.2 Establishment of the finite element model

In Mimics 21 software, finite element modeling differentiates between tooth and bone tissues on the basis of their distinct grayscale values, adjusting thresholds for each tissue type through threshold selection. The selected bone threshold values for this study range from 868 to 5803, whereas the tooth threshold values range from 1300 to 5803. A preliminary three-dimensional model of the cranial maxilla and maxillary dentition is established. Referring to the positions and trajectories of the sutures in the CT images, corresponding bone junctions are selected for offsetting and Boolean operations to construct a 0.5 mm suture, including the palatine midline suture, nasomaxillary suture, frontonasal suture, left and right zygomaticomaxillary sutures, left and right zygomaticotemporal sutures, left and right pterygomaxillary sutures, left and right nasomaxillary sutures, and left and right zygomaticofrontal sutures, for a total of 13 sutures[20]. The outer surface of the maxillary tooth roots was uniformly moved laterally by 0.2 mm, and a periodontal ligament model was obtained through Boolean operations[24–28]. Using the offset command, the maxillary bone was moved inward by 1.3 mm, and then models of cortical and cancellous bones were established through Boolean operations and assembled onto the cranial maxillary bone and dental arch model. On the basis of this established cranial maxillary bone complex model, the Young's modulus of the sutures was set to 500 MPa and 0.68 MPa in Ansys Workbench 2019 software, establishing finite element models of the cranial maxillary bone complex with partially fused and unfused sutures[29, 30]. In Siemens NX 1911 software, a model of the expander was created on the basis of the MSE solid structure and the traditional Hyrax expander, and the established MSE expander model was assembled with the aforementioned cranial maxillary bone complex model. Four experimental models were established, as shown in Fig. 1. Model A is the unfused MARPE model with 337,025 elements and 626,682 nodes; Model B is the partially fused MARPE model with the same number of elements and nodes; Model C is the unfused RME model with 294,169 elements and 556,655 nodes; Model D is the partially fused RME model with the same number of elements and nodes.

To achieve greater simulation accuracy in this study, the craniofacial bones and sutures are set to bonded contact; the expander and the mini-screw implants are also set to bonded contact; the palatal bone and implants are in bonded contact; the tooth roots and periodontal ligament are in bonded contact; and adjacent teeth are designed to have frictional contact. According to previous studies[23, 30], the region around the foramen magnum of the occipital bone is set to zero rotation and zero displacement.

2.3 Material property setting and meshing

In Ansys Workbench 2019 software, the mechanical properties of the materials for the model were assigned on the basis of previous literature. According to prior research, the elastic properties of different tissue structures in the models have specific Young's modulus ratios and Poisson's ratios, as

shown in Table 1[5, 21, 23, 31]. In this study, teeth, craniofacial bones, sutures, periodontal ligaments, mini screws, and expanders were considered continuous, homogeneous, isotropic linear elastic bodies. In this study, a tetrahedral ten-node model was utilized for meshing, as it has been demonstrated to facilitate enhanced stress transmissibility[32]. A primary finding of the study pertains to the mesh delineation of craniofacial bones, teeth, periodontium, and bone joints within the range of 0.5–4 mm, ensuring superior accuracy (see Table 2 for further details).

Table 1
Material properties for each model

model	Young's modulus(MPa)	Poisson's ratio
Bone: Cortical bone; Alveolar bone	13700	0.3
periodontal membrane	0.69	0.49
enamel	20700	0.3
Cancellous bone	1370	0.3
stainless steels	2.e + 005	0.3

Table 2
Mesh sizes for each model

model	Mesh size(mm)
Skeleton	4.0
periodontal membrane	0.5
enamel	2.0
crevice	0.5
micro-implant	0.5

2.4 Coordinate system setting

This study established two coordinate systems. One is for analyzing the stress, strain, and displacement of the jawbone: the X-axis is perpendicular to the sagittal direction (horizontal), with the X-axis pointing to the left of the model for positive values and to the right for negative values; the Y-axis is perpendicular to the coronal plane (sagittal), with the Y-axis pointing backward for positive values and forward for negative values; the Z-axis is perpendicular to the horizontal direction (vertical), with the Z-axis perpendicular to the orbital-ear plane, pointing upward for positive values and downward for negative values to analyze the stress, strain, and displacement of the bone block.

The other coordinate system is for analyzing the stress, strain, and displacement of the teeth: the X-axis represents the mesio-distal direction of the teeth, with the X-axis pointing mesially for positive values and distally for negative values; the Y-axis represents the buccal-lingual direction, with the Y-axis pointing

toward the lingual (palatal) side for positive values and the buccal (cheek) side for negative values; the Z-axis represents the vertical direction, with the Z-axis pointing downward for compression as positive values and upward for extension as negative values.

2.5 Measuring markers

The measurement points along the palatal suture are marked as shown in Fig. 2: the posterior part of the palatal suture is labeled 1, and the anterior part is labeled 2. Starting from point 1, forty-seven evenly distributed points are selected between points 1 and 2 along the line segment, and their transverse displacements are measured. The measurement landmarks for the dental crowns are defined as the midpoint of the incisal edge for the incisors, the cusp tips for the canines, the buccal and palatal cusps for the premolars, and the mesial-distal buccal and mesial-distal palatal cusps for the molars. The landmarks for the dental roots include the apical points of the roots for the incisors, canines, and premolars; the mesial-distal buccal and palatal root apices for the first molars; and the buccal and palatal root apices for the second molars. The tooth point designations are as follows: C for crown, B for the buccal/labial side, P for the palatal side, M for the mesial side, and D for the distal side, as illustrated in Fig. 3.

2.5 Model loading

Referring to previous finite element studies on maxillary arch expansion and clinical practice, this study analyzed the stress distribution and displacement trend of the jawbone, teeth and periodontal membrane with spiral activation of 0.25 mm forced lateral displacement to make the experimental results closer to those of clinical practice[5, 33, 34].

3. Results

3.1 Displacement of and stress on the midpalate suture

The transverse displacements of each marked point on the midpalate joint following stress loading were meticulously recorded and subsequently arranged in a statistical table, as illustrated in A of Fig. 3. The lateral displacement of the palatal raphe in Model A was slightly larger than that in Model B, Model C was significantly larger than that in Model D, and Models A and B were significantly larger than those in Model C and Model D. Model A and Model B palatal median sutures were closer to parallel expansion, and the front was slightly larger than the back. The opening trends of the palatal media in Models C and D were large at the front and small at the back. The left and right palatal media of the four models were not completely symmetrically expanded. The stress distribution trend of the palatal center suture was similar to that of Model A and Model B, and that of Model C was similar to that of Model D. The equivalent stress of Model B > Model A > Model D > Model C, Model A was obviously smaller than that of Model B, Model C was slightly smaller than that of Model D, and the stress distributions of the left and right palatal raphe were not completely symmetric.

3.2 Fracture strain analysis

The strain of the bone sutures was analyzed, as shown in Fig. 4. The equivalent strain produced by the left and right pterygoid maxillary sutures in Model A was the greatest. The strains produced by the other bone sutures except the nasofrontal suture were Model A > Model B > Model C > Model D. The nasofrontal suture in Model C presented the greatest strain, with the maximum strain in Model B occurring in the nasofrontal suture relative to that in Model A. However, the range of strain produced by the nasofrontal suture was diminished, and the strains produced by all the bone sutures in Model D were minimal.

3.3 Cranial maxillary stress distribution and displacement trend

Equivalent stresses and displacements were analyzed for the cranial maxilla, with red showing the areas of greatest stress concentrations or displacements and blue showing the areas of least stress concentrations or displacements. Figure 5 and Fig. 6 show that the craniofacial complexes of Models A and B presented significantly elevated stress levels compared with those of Models C and D. In contrast, the range of stress concentration in Model B was lower than that in Model A, and the magnitude of the stress values exhibited a notable increase. The distribution of stress concentration areas was similar between Model C and Model D, with the greatest concentration observed in the periorbital, nasal, and buccal alveolar bone of the supporting teeth. Model D exhibited higher stress values in these areas than Model C did. The maximum stress distribution between Model A and Model B was observed near the four implant nails, with Model B displaying higher stress values than Model A did. Model B also presented greater stress.

concentration in the palatal bone area surrounding the implant nails. The results demonstrated that Models C and D presented elevated stress concentrations in the alveolar bone in the vicinity of the supporting teeth. All three models (A, B, and C) exhibited substantial lateral displacement, whereas Model D demonstrated comparatively minor lateral displacement. The four models exhibited a backward sagittal displacement trend, with outward and backward displacement.

3.4 Mechanical distribution characteristics and equivalent stress analysis of tooth roots and periodontal hydrostati cpressure

Models A and B had similar trends in the distribution of equivalent force, which was mainly concentrated in the maxillary first molar, with the maximum equivalent force distributed in the root bifurcation of the maxillary first molar. Models C and D had similar trends in the distribution of stress, which was mainly concentrated in the maxillary first premolar and the first molar, with the maximum equivalent force distributed in the palatal region of the cervical part of the first premolar (Fig. 7A).

The analysis of the stress distribution of the roots revealed that the branch resistant teeth of Models C and D were subjected to the greatest stress, with Model D exhibiting a greater stress level than Model C. Similarly, the first molars of Models A and B presented the highest stress levels, with Model B exhibiting a significantly greater stress level than Model A. The equivalent stresses on the roots of the first molars were found to be in the order of Model D > Model B > Model C > Model A. Additionally, the stresses on the roots of the first molars were greater than those on the roots of the second molars (Fig. 7B).

In this study (Fig. 7C), we calculated and analyzed the maximum hydrostatic compressive stress of the periodontal membrane of the maxillary right dentition, which was negatively correlated with compressive stress. The maximum hydrostatic compressive stress of the periodontal membrane of the remaining teeth in the four models, in addition to those of the supporting teeth, were greater than − 0. The maximum hydrostatic compressive stress of the periodontal membrane of the first molar of Model A was also greater than − 0.0047 MPa, whereas the maximum hydrostatic stresses on the periodontal membrane of the first molar of Model B, the first premolar of Model C, and the first molar of Model D were all less than − 0.0047 MPa. The magnitude of the first molar periodontal hydrostatic stress was as follows: Model D presented the greatest value, followed by Model B, Model C, and Model A. The magnitude of the first premolar periodontal hydrostatic stress was as follows: Model D presented the greatest value, followed by Model C, Model B, and Model A.

3.5 Analysis of three-dimensional displacement of tooth marks

The displacement of crowns and roots in the X-axis of Models A, B, and C(Fig. 8) exhibited a consistent trend, whereas the displacement of crowns and roots of maxillary molars in Model D displayed an opposite trend. The displacement of crowns and roots on the X-axis was found to be consistent across all four models, with Model A exhibiting the greatest displacement, Model B demonstrating the least, Model C showing intermediate values, and Model D displaying the most significant displacement. Additionally, the crown—root ratio was the smallest in Model A and the largest in Model D, which presented a significantly larger ratio than did the other three models. Model B also demonstrated a larger ratio than Model C did, with both models displaying ratios that were slightly larger than those observed in Model A. The four models exhibited a uniform trend of displacement on the Y-axis, with all four models displaying negative values along the Y-axis. This was indicative of a distal movement of the tooth toward the middle of the tooth. Model A exhibited the greatest magnitude of displacement, followed by Model B, Model C, and Model D. Model A was found to be significantly larger than the other three models. The crowns and roots of the molars in Model A exhibited movement in the positive direction of the Z-axis, which was characterized by tooth depression. In contrast, the right molars in Model B moved in the negative direction of the Z-axis, which was characterized by tooth elongation. The left molars in this model moved in the positive direction of the Z-axis, which was characterized by depression. The molars in Models C and D also moved along the negative direction of the Z-axis, which was characterized by tooth elongation. The crowns and roots of the anterior teeth of all four models exhibited negative movement along the Z-axis, indicative of elongation of the crowns. Uneven movement of the buccal and

palatal cusps of the supported teeth was observed in all four models on the Z-axis, which suggests that the supported teeth may exhibit a tendency toward buccal inclination.

4. Discussion

4.1 Properties of the Bone Suture Material

The bony suture is a fibrous tissue used to connect the bones of the craniofacial region, helps to act as a shock absorber during impact [35–37], and plays a more important role in craniofacial growth and development. Exogenous forces acting on the maxilla are transmitted through the bone seam to structures farther from the craniofacial region, resulting in mechanical stresses. Owing to the limitations of the previous state-of-the-art methods, some researchers[38] have attempted to construct the bone seam on the maxillary model without assigning its material properties and set it as a discontinuous unit. More satisfactory research results were obtained by assuming that the bone seam was linear in the constructed model. [30, 39, 40]When linear bone joints are assumed in the models developed, more satisfactory results can be obtained. In the present study, the elastic modulus of the bone suture was estimated on the basis of connective and bone tissues and was simulated with Young's modulus (MPa) and Poisson's ratio, and the suture was set to have the mechanical properties of linear elasticity[5, 29]. The degree of fusion of the bone suture affects the biological properties of the material, and the material properties of the craniofacial bone suture vary depending on the degree of ossification; previous studies have revealed that different degrees of ossification of the bone suture result in different displacements of different structures[41, 42]. In some finite element studies[29, 43, 44], the researchers constructed models by varying the elastic modulus of the bone suture material to simulate different degrees of bone suture fusion. Therefore, in this study, the elastic modulus of the bone suture was set at 0.68 MPa and 500 MP to construct the craniofacial complex model to simulate the unfused and partially fused bone sutures, respectively, with reference to previous studies. Since the present study only simulated the force of maxillary expansion once and the change in stress was found to be insignificant in the fully fused model, a fully fused model can be developed in the future to further investigate the effect of the degree of fusion of the bony sutures on the expansion of the arch.

4.2 Osseointegration degree

The resistance observed during maxillary expansion mainly originates from the midpalatal suture and the surrounding bone suture, and the expander increases the maxillary width by separating the midpalatal suture and the surrounding bone suture, thus achieving the purpose of treating MTD. Expansion forces promote the bone remodeling process of the crestal suture [45, 46], whereas cyclic loads such as mastication affect the formation process of the crestal suture [47, 48]. Different spreaders produce different spreading results for different degrees of suture fusion, so assessing the degree of suture fusion is important in choosing the spreading method and timing of spreading. In infancy, the midpalatal suture does not fuse[49], and it is generally accepted that with age, the midpalatal suture

gradually develops right posterior to anterior ossification fusion[50]. There are morphological changes in the midpalatal suture during growth and fusion; the midpalatal suture is an unfused morphology that manifests as a straight line in the first few years of life, and generally, after the age of 15 years, it tends to ossify and fuse to form interlocking and interlocking morphologies[51]. With the increasing number of clinical applications of CBCT, many researchers have staged the midpalatal suture by observing its morphologic features using CBCT to explore the distribution of physiologic age at different stages [30, 52]. However, individual differences in the degree of fusion of the midpalatal suture have also been reported, and incomplete fusion of the midpalatal suture can be found even in adults[53, 54]. In addition, although it is generally accepted that the palatal suture is completely fused in adults aged 20–25 years, the degree of fusion cannot be determined by age alone, and CBCT is still needed to determine the fusion status of the palatal suture when choosing the treatment plan and timing for patients with maxillary transverse hypoplasia. In MTD patients with unfused palatal sutures, traditional tooth-supported expanders can transmit orthopedic forces through the abutment teeth to the jawbone, opening the palatal suture and increasing the maxillary width. As ossification of the midpalatal suture increases, traditional tooth-supported expanders produce more side effects, leading to an increased failure rate. The emergence of MARPE, anchored to the maxillary palate by implant nails, increases the strength of the bony spreading arch and offers the possibility of increasing maxillary width in adolescents with a high degree of midpalatal suture fusion as well as in adults with transverse maxillary hypoplasia[55, 56]. However, there are fewer MARPE studies on the biomechanical characteristics, efficacy, and long-term stability of MTD patients with varying degrees of suture fusion. In future studies, researchers can further refine the analysis of the degree of fusion by CBCT and digitally simulate a biomechanical analysis of different degrees of fusion by altering the material properties to more accurately model the different degrees of fusion.

4.3 Influence of MARPE and RME bow expansion on the midpalatal seam

The morphology and magnitude of displacement of the midpalatal suture opening are usually used clinically to evaluate the effect of maxillary expansion, and many studies have revealed that the midpalatal suture is almost parallel to the opening after MARPE [57–59] and that the midpalatal suture is wedge-shaped after RME [60, 61]. In the present study, by measuring the transverse displacement of points on the midpalatal crease, it was found more intuitively that the midpalatal crease was more similar to a parallel widening after reaming for MARPE than to an anterior and posterior V-shaped widening after reaming for RME, which is consistent with the results of most studies. The difference in the midpalatal crease opening pattern between the two expanders may be due to the different biomechanical principles of the two expanders. MARPE typically involves the use of two or four implants anchored to the posterior portion of the palatal bone so that the orthopedic forces generated by the expansion of the arch are applied directly to the palatal bone and distributed along the midpalatal crease, promoting more parallel widening of the midpalatal crease. In addition, during MARPE, the nails implanted are usually fixed with two layers of bone cortex, which can increase the stability of the nails

and reduce the likelihood of deformation and fracture of the nails, thus promoting more parallel widening of the palatal fold[62, 63]. In this study, we measured the transverse displacement of the right and left midpalatal sutures and found that the midpalatal sutures were asymmetrically widened and that there were differences in the amount of stress on the right and left midpalatal sutures. The cause of asymmetric widening of the midpalatal suture is not well understood, and it was found that regardless of the MARPE design, almost half of the patients did not always have symmetric widening in the transverse direction, and that patients with an asymmetric initial position of the midpalatal suture had a higher chance of having asymmetric widening of the midpalatal suture[64].Asymmetric widening of the midpalatal suture may also be related to external forces, such as unilateral retrognathia that restricts maxillary movement on one side, resulting in asymmetric widening of the midpalatal suture, and more clinical and biomechanical studies are needed to explain the cause of asymmetric widening of the midpalatal suture. Angelieri et al.[52] found that the D stage showed greater widening, and the results of this study are similar to the clinical findings of Angelieri et al. In this study, we found that as the degree of fusion of the midpalatal suture increased, the morphology of the opening of the midpalatal suture during MARPE and RME was similar to that of the unfused suture, but the flaring of the midpalatal suture decreased, and the magnitude of the decrease during RME was significantly greater than that during MARPE, and the stresses exerted on the midpalatal suture were significantly increased, which can be interpreted by stress analysis to mean that with the increase in resistance to opening of the midpalatal suture, the orthopedic forces generated by the flaring of the arch are applied more to the resistance of the midpalatal suture to the stringer.

4.4 Skeletal and Dental Effects of MARPE and RME of the Arch

For the clinical treatment of patients with lateral maxillary underdevelopment, there is a need to achieve more osseous effects and reduce the likelihood of dental side effects. In this study, we found that the maximum stress distributed during MARPE was mainly concentrated near the implant nails in the maxillary palate, which is consistent with the results of many finite element studies[65, 66], and the stresses generated during MARPE in the craniofacial bone and the displacement of the maxilla in all three directions were significantly greater than those during RME, possibly because the implant nails provide greater support resistance during the expansion process, which transmits the orthopedic force of expansion directly to the bone, producing a greater bone effect. In contrast, the stress concentration in the alveolar bone on the buccal side of the supporting teeth was greater during RME, which may be the cause of alveolar bone bending during RME [67, 68]. In addition, this study revealed that as the degree of bone fusion increased, the stress generated by MARPE near the maxillary implant nails increased, and the stress in the per-maxillary bone tissue also increased slightly, suggesting that our implant nails can generate greater orthopedic force to expand the maxilla and that at the same time, there may be stress overload that leads to deformation and loosening, which should be closely observed in clinical settings. In contrast, as the degree of bone fusion increases, craniofacial bone stress decreases after RME, but the stress on the buccal side of the tooth bone of the supporting teeth increases significantly, which may

explain why patients with a greater degree of bone fusion have greater alveolar bone curvature after arch expansion with RME. Copello et al.[29] compared the effects of MARPE and RME on buccal alveolar bone thickness and marginal alveolar bone and reported that, compared with MARPE, conventional RME may result in greater bone thickness loss[69] and buccal tilting of the supporting teeth after RME for arch expansion, whereas MARPE reduces the likelihood of this side effect[13, 70, 71]. Furthermore, in addition to differences in the type of appliance and the degree of osseointegration, the design of the appliance, the quality of the appliance material and welds, the size of the microimplant nails, the single layer of cortical fixation or bilateral cortical fixation, and the number of arch expansion activations may lead to adverse side effects that cause buccal movement of the teeth[17]. In this study, we found that both MARPE and RME produced buccal tilting movement of the teeth by measuring the lateral displacement of the crowns and roots and the crown—root ratio, respectively, and this result is consistent with the study of Lagravère et al.[72]. In addition, we found that the buccal tilting movement of the teeth after MARPE was significantly less than that after RME. As the degree of fusion of the osseous suture increased, the degree of buccal tilting of the teeth increased, and the RME increased by a greater amount, suggesting that in patients with a high degree of osseous fusion, RME has a greater risk of bone dehiscence and bone dehiscence.

Vertical control has always been an issue that orthodontists pay close attention to in clinical practice, and once the vertical direction is out of control, it can lead to aesthetic problems such as deterioration of the facial shape, especially in patients with high angles and their disadvantages. In the present study, we found that more elongation of the molars was observed in the Z-axis of the RME expansion model; the molars in the MARPE expansion model tended to be depressed, and the slight elongation of one side of the molars with the increase in the degree of fusion of the bone sutures may be due to the asymmetry of the initial two sides of the maxillary model, which resulted in asymmetry in the conduction of the orthopedic force of the expanded arch. The key to successful adult expansion is to apply effective orthopedic forces to the midpalatal suture of the maxilla to produce a large bony effect with few dental side effects. Therefore, the results of this study and previous studies[8, 13, 62, 66] suggest that MARPE may be more appropriate for late adolescent and young MTD patients with a high degree of suture fusion, which can produce a greater osseous effect but still has a dental effect, and that tooth movement should also be closely monitored clinically. On the basis of clinical observations and individual differences, MARPE may still require appropriate overcorrection in clinical practice.

4.5 Influence of MARPE and RME on periodontal tissues

The periodontal ligament (PDL), along with bone tissue, is the supporting tissue for teeth and is subjected to many forms of stress during orthodontic treatment [73]. Finite element analysis has been shown to be a noninvasive method that can analyze the distribution of mechanical stresses on the periodontium after the application of orthodontic forces[74]. In many studies, researchers have used finite element analysis to analyze and evaluate the biomechanical properties of the PDL in various simulation scenarios, and commonly used measures include equivalent stress[24, 75–81] (von Mises

equivalent stress) and periodontal hydrostatic pressure[80, 82–85]. In vascularized dental tissues, the presence of higher hydrostatic pressures causes ischemia, necrosis, and further loss of periodontal tissue, but in less vascularized tissues, such as teeth and bone, the presence of higher hydrostatic pressures may not result in more significant tissue loss[86]. If the hydrostatic pressure on the periodontium exceeds the capillary pressure in the area, circulatory disturbances will occur, increasing the risk of root resorption[87]. Therefore, the value of hydrostatic stress in the periodontium can also be an indicator of root resorption. According to previous studies, the threshold value of capillary pressure in the PDL was found to be 0.0047 MPa, and there is a risk of root resorption when the hydrostatic stress is greater than 0.0047 MPa[82, 87, 88]. In this study, we analyzed the effects of MARPE and RME on periodontal tissues by measuring the hydrostatic pressure of the periodontium and the equivalent force of the periodontium and reported that the hydrostatic stresses on teeth in the MARPE model with nonfused bone sutures were less than 0.0047 MPa, whereas the hydrostatic stresses on the periodontium of the supporting teeth in the MARPE model with partially fused bone sutures were greater than 0.0047 MPa, indicating a risk of root resorption. The magnitude of hydrostatic stress in the periodontium of the supported teeth in both the unfused and the fused RME models was greater than 0.0047 MPa, and the hydrostatic stress in the periodontium of the supported teeth in the MARPE model was much lower than that in the RME model under the same conditions. These findings suggest that the risk of root resorption in supported teeth increases with increasing bone fusion after MARPE and RME, but the risk of root resorption in supported teeth after MARPE for arch expansion is lower than that after RME. In this study, we found that the periodontal equivalent force was greater in the supported teeth than in the remaining teeth after both MARPE and RME. As the degree of fusion increased, the equivalent force on the supported teeth increased, and the stress after MARPE was less than that after RME, which is consistent with the trend of the hydrostatic stress distribution. This result is consistent with the hydrostatic stress distribution. These findings suggest that MARPE may be more suitable for young MTD patients with a high degree of osseointegration and that we should pay attention to the root condition of the supporting teeth and apply light forces in clinical practice.

Declarations

Ethics approval and consent to participate

Shenyang Stomatological Hospital (Ethics Code: 2022010). This study was conducted in accordance with the principles of the Helsinki Declaration (World Medical Association, 2013). Participants signed written informed consent forms before joining the study. The research plan has been approved by the Medical Ethics Committee of Shenyang Stomatological Hospital (ethics batch number: 2022010). Registration date: September 22, 2022.

Consent for publication

No individual participant data or identifying information is included in this manuscript, so consent for publication is not applicable.

Availability of data and materials

Study data are clinical patient data that cannot be made openly available. For inquiries

about the data and collaborations please contact the corresponding author.

Competing Interests

All authors declare no competing interests.

Funding

All authors are from the Shenyang Science and Technology Plan Project, titled "Digital Precision Diagnosis and Treatment of Maxillary Underdevelopment" (Project No. 21-173-9-11).

Authors' contributions

YeYa Yuan: Conceptualization, ideas, research goals and aims, resources, supervision, creation of models.

HaoPeng Wu: Data curation, writing original draft, methodology development or design of methodology, creation of models and should be considered co-first author.

Bing Liu:Methodology development or design of methodology, research goals and aims, software programming, software development, designing computer programs

NingNing Wang:Resources, supervision, methodology development or design of methodology.

YueMei Sun:funding acquisition ,acquisition of the financial support for the project leading to this publication.

JieYu Yang:involving in data acquisition and analysis.

Xin Li: contributing to analysis, interpretation, and critical revision of the manuscript.

HaoQing Zhang contributing to analysis, interpretation, and critical revision of the manuscript.

JiHui Liu : Data curation, writing original draft, software programming, software development, investigation conducting a research and investigation process, designing computer programs, should be considered corresponding author.

References

1. NEYT N M, MOMMAERTS M Y, ABELOOS J V, et al. Problems, obstacles and complications with transpalatal distraction in non-congenital deformities [J]. J Craniomaxillofac Surg, 2002, 30(3): 139-43.

2. RAMIRES T, MAIA R A, BARONE J R. Nasal cavity changes and the respiratory standard after maxillary expansion [J]. Braz J Otorhinolaryngol, 2008, 74(5): 763-9.
3. DA SILVA FILHO O G, SANTAMARIA M, JR., CAPELOZZA FILHO L. Epidemiology of posterior crossbite in the primary dentition [J]. J Clin Pediatr Dent, 2007, 32(1): 73-8.
4. BRUNELLE J A, BHAT M, LIPTON J A. Prevalence and distribution of selected occlusal characteristics in the US population, 1988-1991 [J]. J Dent Res, 1996, 75 Spec No: 706-13.
5. GUPTA V, RAI P, TRIPATHI T, et al. Stress distribution and displacement with four different types of MARPE on craniofacial complex: A three-dimensional finite element analysis [J]. Int Orthod, 2023, 21(4): 100813.
6. VILLA M P, RIZZOLI A, MIANO S, et al. Efficacy of rapid maxillary expansion in children with obstructive sleep apnea syndrome: 36 months of follow-up [J]. Sleep Breath, 2011, 15(2): 179-84.
7. JAFARI A, SHETTY K S, KUMAR M. Study of stress distribution and displacement of various craniofacial structures following application of transverse orthopedic forces--a three-dimensional FEM study [J]. Angle Orthod, 2003, 73(1): 12-20.
8. CHOI S H, SHI K K, CHA J Y, et al. Nonsurgical miniscrew-assisted rapid maxillary expansion results in acceptable stability in young adults [J]. Angle Orthod, 2016, 86(5): 713-20.
9. CHAMBERLAND S. Maxillary expansion in nongrowing patients. Conventional, surgical, or miniscrew-assisted, an update [J]. J World Fed Orthod, 2023, 12(4): 173-83.
10. ABATE A, LANTERI V, MARCOLONGO L, et al. Evaluation of Masticatory Muscles in Adult Patients with Maxillary Hypoplasia Treated with Surgically Assisted Rapid Maxillary Expansion (SARME): A Retrospective Study [J]. J Clin Med, 2023, 12(2).
11. LI K, GUILLEMINAULT C. Surgical and non-surgical maxillary expansion: expansion patterns, complications and failures [J]. Orthod Fr, 2022, 93(Suppl 1): 35-46.
12. SYGOUROS A, MOTRO M, UGURLU F, et al. Surgically assisted rapid maxillary expansion: cone-beam computed tomography evaluation of different surgical techniques and their effects on the maxillary dentoskeletal complex [J]. Am J Orthod Dentofacial Orthop, 2014, 146(6): 748-57.
13. LEE K J, PARK Y C, PARK J Y, et al. Miniscrew-assisted nonsurgical palatal expansion before orthognathic surgery for a patient with severe mandibular prognathism [J]. Am J Orthod Dentofacial Orthop, 2010, 137(6): 830-9.
14. BRUNETTO D P, SANT'ANNA E F, MACHADO A W, et al. Non-surgical treatment of transverse deficiency in adults using Microimplant-assisted Rapid Palatal Expansion (MARPE) [J]. Dental Press J Orthod, 2017, 22(1): 110-25.
15. LIN L, AHN H W, KIM S J, et al. Tooth-borne vs bone-borne rapid maxillary expanders in late adolescence [J]. Angle Orthod, 2015, 85(2): 253-62.
16. NOJIMA L I, NOJIMA M, CUNHA A C D, et al. Mini-implant selection protocol applied to MARPE [J]. Dental Press J Orthod, 2018, 23(5): 93-101.

17. OLIVEIRA P L E, SOARES K E M, ANDRADE R M, et al. Stress and displacement of mini-implants and appliance in Mini-implant Assisted Rapid Palatal Expansion: analysis by finite element method [J]. Dental Press J Orthod, 2021, 26(4): e21203.
18. AHMIDA A, MEHTA S, AMELEMAH E, et al. Short-term and long-term effects of miniscrew-assisted and conventional rapid palatal expansion on the cranial and circummaxillary sutures [J]. Am J Orthod Dentofacial Orthop, 2023, 163(4): e115-e26.
19. PAVLIN D, VUKICEVIC D. Mechanical reactions of facial skeleton to maxillary expansion determined by laser holography [J]. Am J Orthod, 1984, 85(6): 498-507.
20. CAPUTO A A, CHACONAS S J, HAYASHI R K. Photoelastic visualization of orthodontic forces during canine retraction [J]. Am J Orthod, 1974, 65(3): 250-9.
21. COZZANI M, NUCCI L, LUPINI D, et al. Two different designs of mini-screw assisted maxillary expanders, using FEM to analyse stress distribution in craniofacial structures and anchor teeth [J]. Int Orthod, 2022, 20(1): 100607.
22. PAN S, GAO X, SUN J, et al. Effects of novel microimplant-assisted rapid palatal expanders manufactured by 3-dimensional printing technology: A finite element study [J]. Am J Orthod Dentofacial Orthop, 2023, 164(5): 700-11.
23. SURESH S, SUNDARESWARAN S, SATHYANADHAN S. Effect of microimplant assisted rapid palatal expansion on bone-anchored maxillary protraction: A finite element analysis [J]. Am J Orthod Dentofacial Orthop, 2021, 160(4): 523-32.
24. GUPTA M, MADHOK K, KULSHRESTHA R, et al. Determination of stress distribution on periodontal ligament and alveolar bone by various tooth movements - A 3D FEM study [J]. J Oral Biol Craniofac Res, 2020, 10(4): 758-63.
25. AHUJA S, GUPTA S, BHAMBRI E, et al. Comparison of conventional methods of simultaneous intrusion and retraction of maxillary anterior: a finite element analysis [J]. J Orthod, 2018, 45(4): 243-9.
26. PIETRZAK G, CURNIER A, BOTSIS J, et al. A nonlinear elastic model of the periodontal ligament and its numerical calibration for the study of tooth mobility [J]. Comput Methods Biomech Biomed Engin, 2002, 5(2): 91-100.
27. WEI Z, YU X, XU X, et al. Experiment and hydro-mechanical coupling simulation study on the human periodontal ligament [J]. Comput Methods Programs Biomed, 2014, 113(3): 749-56.
28. ZHU J, RONG Q, WANG X, et al. Influence of remaining tooth structure and restorative material type on stress distribution in endodontically treated maxillary premolars: A finite element analysis [J]. J Prosthet Dent, 2017, 117(5): 646-55.
29. PROVATIDIS C G, GEORGIOPOULOS B, KOTINAS A, et al. Evaluation of craniofacial effects during rapid maxillary expansion through combined in vivo/in vitro and finite element studies [J]. Eur J Orthod, 2008, 30(5): 437-48.
30. MACGINNIS M, CHU H, YOUSSEF G, et al. The effects of micro-implant assisted rapid palatal expansion (MARPE) on the nasomaxillary complex--a finite element method (FEM) analysis [J]. Prog

Orthod, 2014, 15(1): 52.

31. BALAKRISHNAN R, SENGOTTUVEL N, ALTAF S K, et al. Three-Dimensional Finite Element Analysis of Maxillary Protraction Using Diverse Modes of Rapid Palatal Expansion [J]. Cureus, 2023, 15(3): e36328.
32. GAUTAM P, VALIATHAN A, ADHIKARI R. Stress and displacement patterns in the craniofacial skeleton with rapid maxillary expansion: a finite element method study [J]. Am J Orthod Dentofacial Orthop, 2007, 132(1): 5.e1-11.
33. MENG W Y, MA Y Q, SHI B, et al. The comparison of biomechanical effects of the conventional and bone-borne palatal expanders on late adolescence with unilateral cleft palate: a 3-dimensional finite element analysis [J]. BMC Oral Health, 2022, 22(1): 600.
34. LEE H, NGUYEN A, HONG C, et al. Biomechanical effects of maxillary expansion on a patient with cleft palate: A finite element analysis [J]. Am J Orthod Dentofacial Orthop, 2016, 150(2): 313-23.
35. BEEDERMAN M, FARINA E M, REID R R. Molecular basis of cranial suture biology and disease: Osteoblastic and osteoclastic perspectives [J]. Genes Dis, 2014, 1(1): 120-5.
36. MALOUL A, FIALKOV J, WAGNER D, et al. Characterization of craniofacial sutures using the finite element method [J]. J Biomech, 2014, 47(1): 245-52.
37. KHONSARI R H, OLIVIER J, VIGNEAUX P, et al. A mathematical model for mechanotransduction at the early steps of suture formation [J]. Proc Biol Sci, 2013, 280(1759): 20122670.
38. IŞERI H, TEKKAYA A E, OZTAN O, et al. Biomechanical effects of rapid maxillary expansion on the craniofacial skeleton, studied by the finite element method [J]. Eur J Orthod, 1998, 20(4): 347-56.
39. LEE H K, BAYOME M, AHN C S, et al. Stress distribution and displacement by different bone-borne palatal expanders with micro-implants: a three-dimensional finite-element analysis [J]. Eur J Orthod, 2014, 36(5): 531-40.
40. LEE H, TING K, NELSON M, et al. Maxillary expansion in customized finite element method models [J]. Am J Orthod Dentofacial Orthop, 2009, 136(3): 367-74.
41. GARDNER G E, KRONMAN J H. Cranioskeletal displacements caused by rapid palatal expansion in the rhesus monkey [J]. Am J Orthod, 1971, 59(2): 146-55.
42. TIMMS D J. A study of basal movement with rapid maxillary expansion [J]. Am J Orthod, 1980, 77(5): 500-7.
43. VERRUE V, DERMAUT L, VERHEGGHE B. Three-dimensional finite element modelling of a dog skull for the simulation of initial orthopaedic displacements [J]. Eur J Orthod, 2001, 23(5): 517-27.
44. TANNE K, HIRAGA J, SAKUDA M. Effects of directions of maxillary protraction forces on biomechanical changes in craniofacial complex [J]. Eur J Orthod, 1989, 11(4): 382-91.
45. LIU S S, OPPERMAN L A, KYUNG H M, et al. Is there an optimal force level for sutural expansion? [J]. Am J Orthod Dentofacial Orthop, 2011, 139(4): 446-55.
46. LI M, ZHANG Z, GU X, et al. MicroRNA-21 affects mechanical force-induced midpalatal suture remodelling [J]. Cell Prolif, 2020, 53(1): e12697.

47. OPPENHEIMER A J, RHEE S T, GOLDSTEIN S A, et al. Force-induced craniosynostosis via paracrine signaling in the murine sagittal suture [J]. J Craniofac Surg, 2012, 23(2): 573-7.
48. PEPTAN A I, LOPEZ A, KOPHER R A, et al. Responses of intramembranous bone and sutures upon in vivo cyclic tensile and compressive loading [J]. Bone, 2008, 42(2): 432-8.
49. BJöRK A. Sutural growth of the upper face studied by the implant method [J]. Acta Odontol Scand, 1966, 24(2): 109-27.
50. PERSSON M, THILANDER B. Palatal suture closure in man from 15 to 35 years of age [J]. Am J Orthod, 1977, 72(1): 42-52.
51. SUZUKI H, MOON W, PREVIDENTE L H, et al. Miniscrew-assisted rapid palatal expander (MARPE): the quest for pure orthopedic movement [J]. Dental Press J Orthod, 2016, 21(4): 17-23.
52. ANGELIERI F, CEVIDANES L H, FRANCHI L, et al. Midpalatal suture maturation: classification method for individual assessment before rapid maxillary expansion [J]. Am J Orthod Dentofacial Orthop, 2013, 144(5): 759-69.
53. NAYA-IMAI H, UCHIDA Y, INABA M, et al. Age dependence of the maturation of the midpalatal suture in the stability of orthodontic anchoring screws [J]. Am J Orthod Dentofacial Orthop, 2022, 161(6): 809-19.
54. KATTI G, SHAHBAZ S, KATTI C, et al. Evaluation of Midpalatal Suture Ossification Using Cone-Beam Computed Tomography: A Digital Radiographic Study [J]. Acta Medica (Hradec Kralove), 2020, 63(4): 188-93.
55. PARK J J, PARK Y C, LEE K J, et al. Skeletal and dentoalveolar changes after miniscrew-assisted rapid palatal expansion in young adults: A cone-beam computed tomography study [J]. Korean J Orthod, 2017, 47(2): 77-86.
56. SIDDHISARIBUTR P, KHLONGWANITCHAKUL K, ANUWONGNUKROH N, et al. Effectiveness of miniscrew assisted rapid palatal expansion using cone beam computed tomography: A systematic review and meta-analysis [J]. Korean J Orthod, 2022, 52(3): 182-200.
57. CANTARELLA D, DOMINGUEZ-MOMPELL R, MALLYA S M, et al. Changes in the midpalatal and pterygopalatine sutures induced by micro-implant-supported skeletal expander, analyzed with a novel 3D method based on CBCT imaging [J]. Prog Orthod, 2017, 18(1): 34.
58. SALMORIA I, DE SOUZA E C, FURTADO A, et al. Dentoskeletal changes and their correlations after micro-implant-assisted palatal expansion (MARPE) in adults with advanced midpalatal suture ossification [J]. Clin Oral Investig, 2022, 26(3): 3021-31.
59. CHO A R, PARK J H, MOON W, et al. Short-term effects of microimplant-assisted rapid palatal expansion on the circummaxillary sutures in skeletally mature patients: A cone-beam computed tomography study [J]. Am J Orthod Dentofacial Orthop, 2022, 161(2): e187-e97.
60. LIONE R, BALLANTI F, FRANCHI L, et al. Treatment and posttreatment skeletal effects of rapid maxillary expansion studied with low-dose computed tomography in growing subjects [J]. Am J Orthod Dentofacial Orthop, 2008, 134(3): 389-92.

61. GHONEIMA A, ABDEL-FATTAH E, HARTSFIELD J, et al. Effects of rapid maxillary expansion on the cranial and circummaxillary sutures [J]. Am J Orthod Dentofacial Orthop, 2011, 140(4): 510-9.
62. LEE R J, MOON W, HONG C. Effects of monocortical and bicortical mini-implant anchorage on bone-borne palatal expansion using finite element analysis [J]. Am J Orthod Dentofacial Orthop, 2017, 151(5): 887-97.
63. LI N, SUN W, LI Q, et al. Skeletal effects of monocortical and bicortical mini-implant anchorage on maxillary expansion using cone-beam computed tomography in young adults [J]. Am J Orthod Dentofacial Orthop, 2020, 157(5): 651-61.
64. ALMAQRAMI B S, ALHAMMADI M S, AL-SOMAIRI M A A, et al. Three-dimensional assessment of asymmetric mid-palatal suture expansion assisted by a customized microimplant-supported rapid palatal expander in non-growing patients: Uncontrolled Clinical Trial [J]. Orthod Craniofac Res, 2022, 25(2): 234-42.
65. HARTONO N, SOEGIHARTO B M, WIDAYATI R. The difference of stress distribution of maxillary expansion using rapid maxillary expander (RME) and maxillary skeletal expander (MSE)-a finite element analysis [J]. Prog Orthod, 2018, 19(1): 33.
66. SEONG E H, CHOI S H, KIM H J, et al. Evaluation of the effects of miniscrew incorporation in palatal expanders for young adults using finite element analysis [J]. Korean J Orthod, 2018, 48(2): 81-9.
67. CHUN J H, DE CASTRO A C R, OH S, et al. Skeletal and alveolar changes in conventional rapid palatal expansion (RPE) and miniscrew-assisted RPE (MARPE): a prospective randomized clinical trial using low-dose CBCT [J]. BMC Oral Health, 2022, 22(1): 114.
68. GARRETT B J, CARUSO J M, RUNGCHARASSAENG K, et al. Skeletal effects to the maxilla after rapid maxillary expansion assessed with cone-beam computed tomography [J]. Am J Orthod Dentofacial Orthop, 2008, 134(1): 8-9.
69. COPELLO F M, MARAñóN-VáSQUEZ G A, BRUNETTO D P, et al. Is the buccal alveolar bone less affected by mini-implant assisted rapid palatal expansion than by conventional rapid palatal expansion?-A systematic review and meta-analysis [J]. Orthod Craniofac Res, 2020, 23(3): 237-49.
70. CHEN R. Effects of rapid maxillary expansion on anchorage alveolar bone meta-analysis [J]. Acta Odontol Scand, 2023, 81(7): 499-507.
71. CARVALHO P H A, MOURA L B, TRENTO G S, et al. Surgically assisted rapid maxillary expansion: a systematic review of complications [J]. Int J Oral Maxillofac Surg, 2020, 49(3): 325-32.
72. LAGRAVèRE M O, CAREY J, HEO G, et al. Transverse, vertical, and anteroposterior changes from bone-anchored maxillary expansion vs traditional rapid maxillary expansion: a randomized clinical trial [J]. Am J Orthod Dentofacial Orthop, 2010, 137(3): 304.e1-12; discussion -5.
73. MOGA R A, OLTEANU C D, BOTEZ M D, et al. Assessment of the Orthodontic External Resorption in Periodontal Breakdown-A Finite Elements Analysis (Part I) [J]. Healthcare (Basel), 2023, 11(10).
74. VIKRAM N R, SENTHIL KUMAR K S, NAGACHANDRAN K S, et al. Apical stress distribution on maxillary central incisor during various orthodontic tooth movements by varying cemental and two different periodontal ligament thicknesses: a FEM study [J]. Indian J Dent Res, 2012, 23(2): 213-20.

75. RUBO J H, CAPELLO SOUZA E A. Finite-element analysis of stress on dental implant prosthesis [J]. Clin Implant Dent Relat Res, 2010, 12(2): 105-13.
76. SHAW A M, SAMESHIMA G T, VU H V. Mechanical stress generated by orthodontic forces on apical root cementum: a finite element model [J]. Orthod Craniofac Res, 2004, 7(2): 98-107.
77. FIELD C, ICHIM I, SWAIN M V, et al. Mechanical responses to orthodontic loading: a 3-dimensional finite element multi-tooth model [J]. Am J Orthod Dentofacial Orthop, 2009, 135(2): 174-81.
78. MERDJI A, MOOTANAH R, BACHIR BOUIADJRA B A, et al. Stress analysis in single molar tooth [J]. Mater Sci Eng C Mater Biol Appl, 2013, 33(2): 691-8.
79. MARAVIĆ T, COMBA A, MAZZITELLI C, et al. Finite element and in vitro study on biomechanical behavior of endodontically treated premolars restored with direct or indirect composite restorations [J]. Sci Rep, 2022, 12(1): 12671.
80. HUANG L, NEMOTO R, OKADA D, et al. Investigation of stress distribution within an endodontically treated tooth restored with different restorations [J]. J Dent Sci, 2022, 17(3): 1115-24.
81. PéREZ-GONZáLEZ A, ISERTE-VILAR J L, GONZáLEZ-LLUCH C. Correction to: Interpreting finite element results for brittle materials in endodontic restorations [J]. BMC Surg, 2023, 23(1): 238.
82. HOHMANN A, WOLFRAM U, GEIGER M, et al. Periodontal ligament hydrostatic pressure with areas of root resorption after application of a continuous torque moment [J]. Angle Orthod, 2007, 77(4): 653-9.
83. WU J, LIU Y, WANG D, et al. Investigation of effective intrusion and extrusion force for maxillary canine using finite element analysis [J]. Comput Methods Biomech Biomed Engin, 2019, 22(16): 1294-302.
84. WU J L, LIU Y F, PENG W, et al. A biomechanical case study on the optimal orthodontic force on the maxillary canine tooth based on finite element analysis [J]. J Zhejiang Univ Sci B, 2018, 19(7): 535-46.
85. LIU X, WANG W, GAO J, et al. Actual contribution ratio of maxillary and mandibular molars for total molar relationship correction during maxillary molar sequential distalization using clear aligners with Class II elastics: A finite element analysis [J]. Am J Orthod Dentofacial Orthop, 2023, 164(4): e106-e20.
86. MOGA R A, OLTEANU C D, BURU S M, et al. Cortical and Trabecular Bone Stress Assessment during Periodontal Breakdown-A Comparative Finite Element Analysis of Multiple Failure Criteria [J]. Medicina (Kaunas), 2023, 59(8).
87. LIU X, CHENG Y, QIN W, et al. Effects of upper-molar distalization using clear aligners in combination with Class II elastics: a three-dimensional finite element analysis [J]. BMC Oral Health, 2022, 22(1): 546.
88. DOROW C, SANDER F G. Development of a model for the simulation of orthodontic load on lower first premolars using the finite element method [J]. J Orofac Orthop, 2005, 66(3): 208-18.

Figures

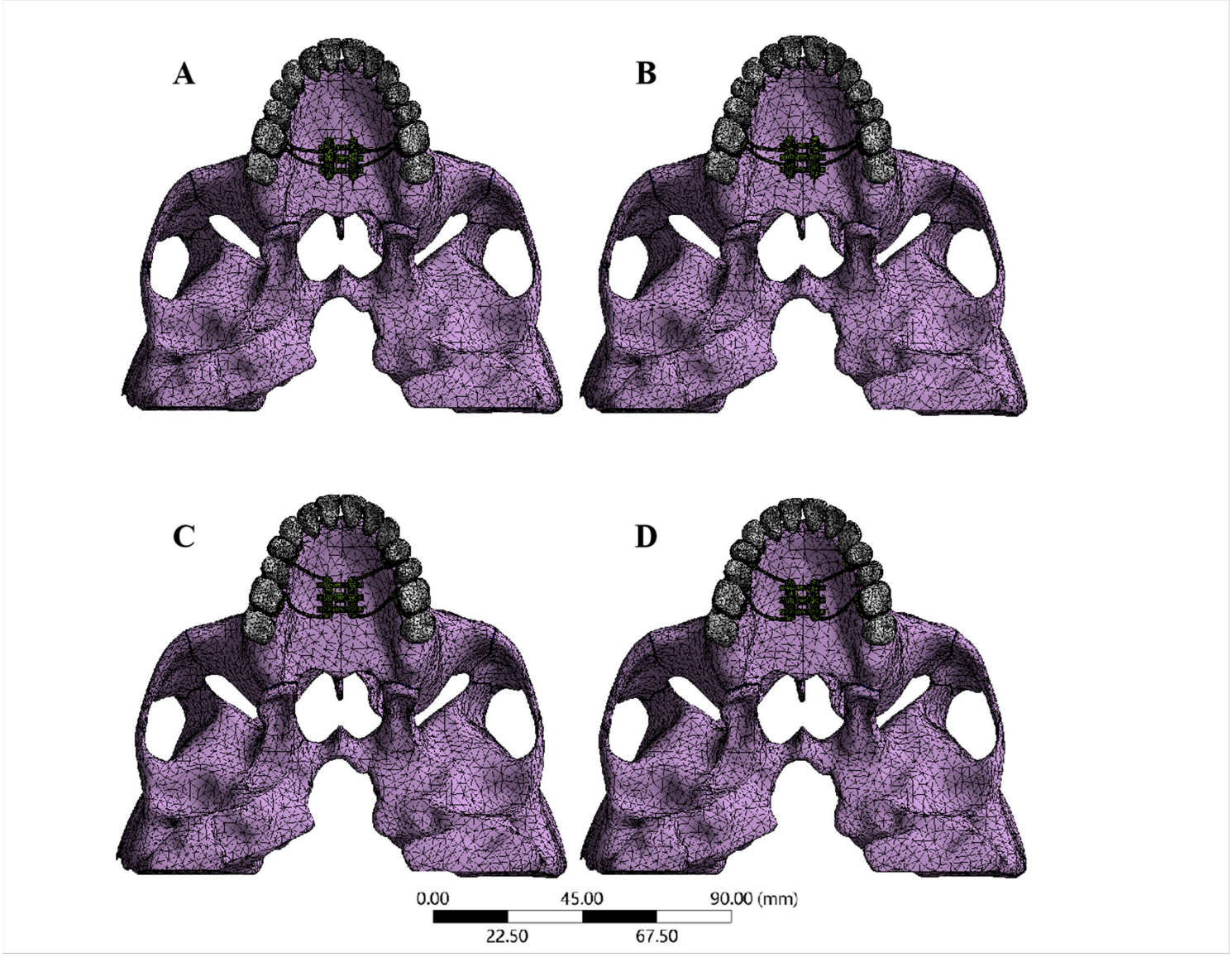


Figure 1

depicts four models of spread bows: Model A is a MARPE bow with unfused bone sutures; Model B is a MARPE bow with partially fused bone sutures; Model C is an RME bow with unfused bone sutures; and Model D is an RME bow with partial suture bone fusion.

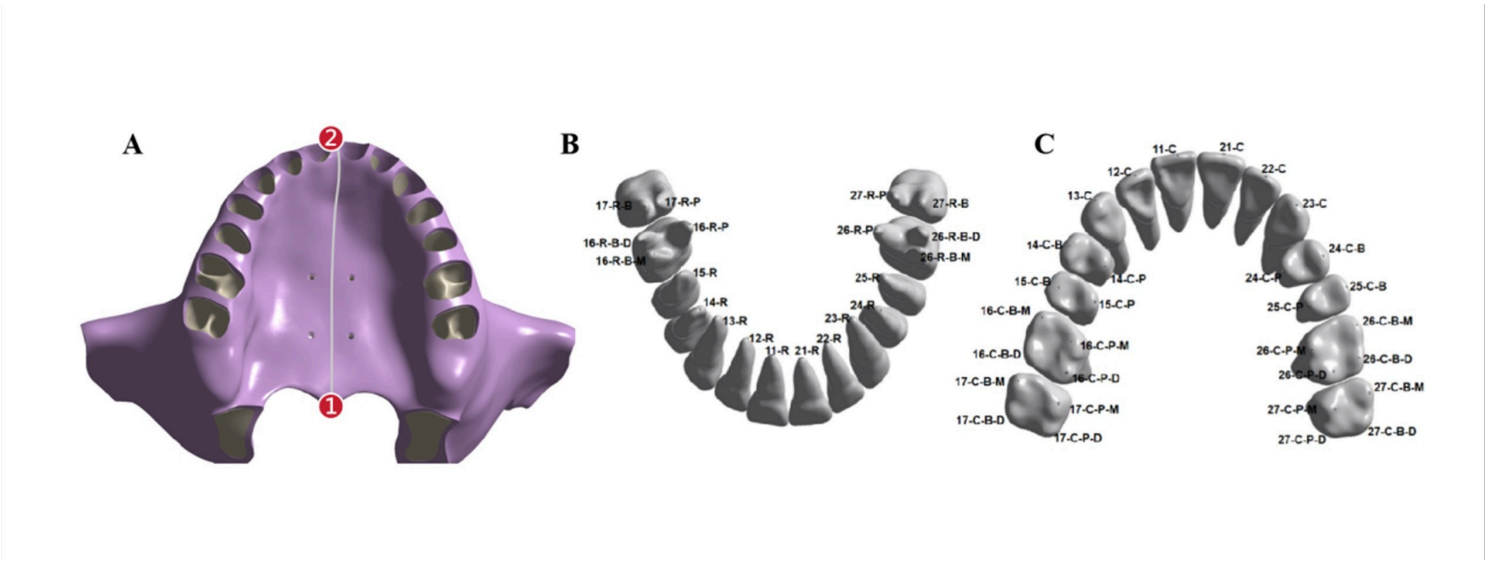


Figure 2

Measurement points in the center seam of the palate and dental measurement markers

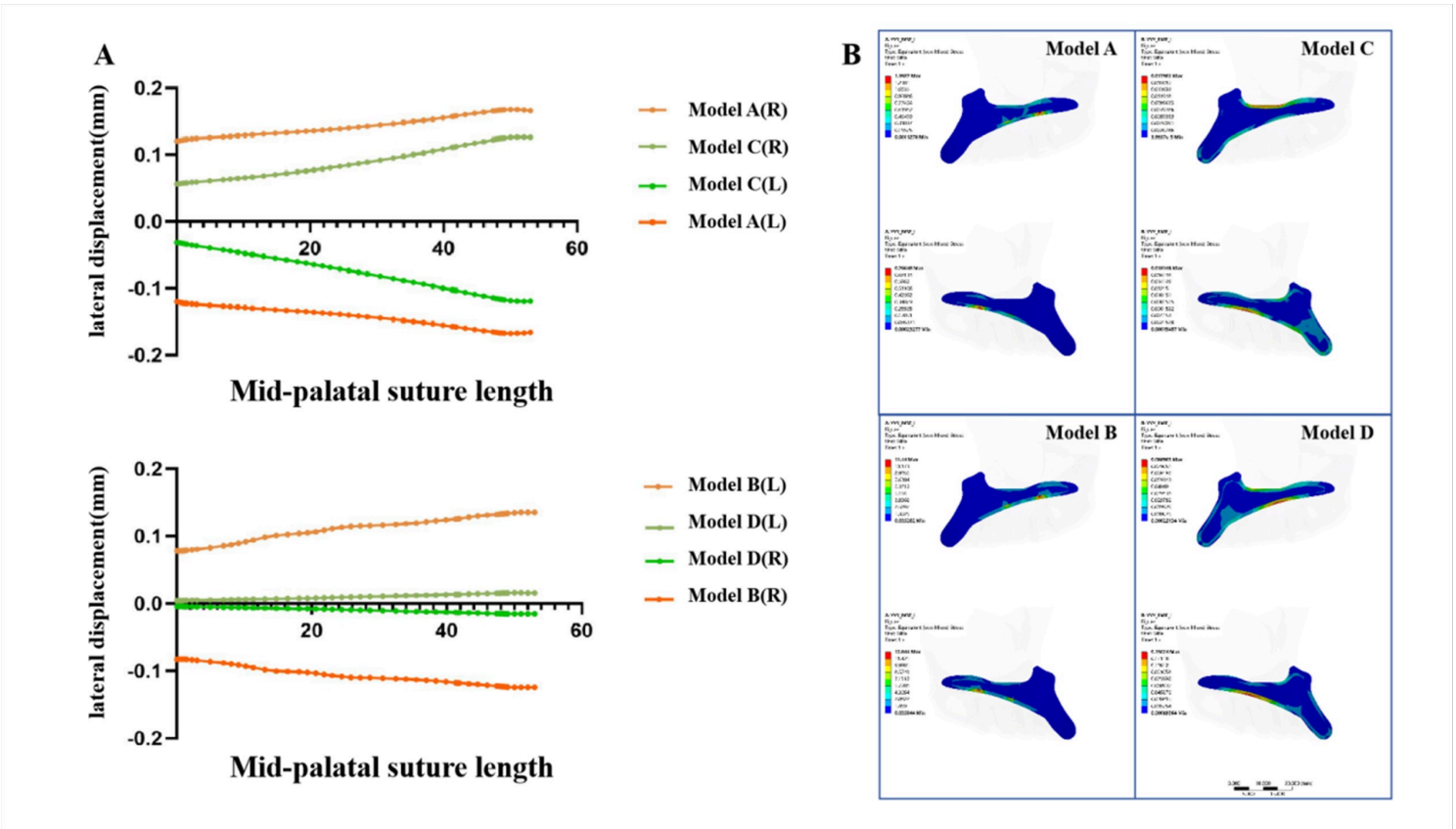


Figure 3

shows the displacement trend and stress distribution of the midpalatal suture following arch expansion, presented in the form of a cloud diagram.

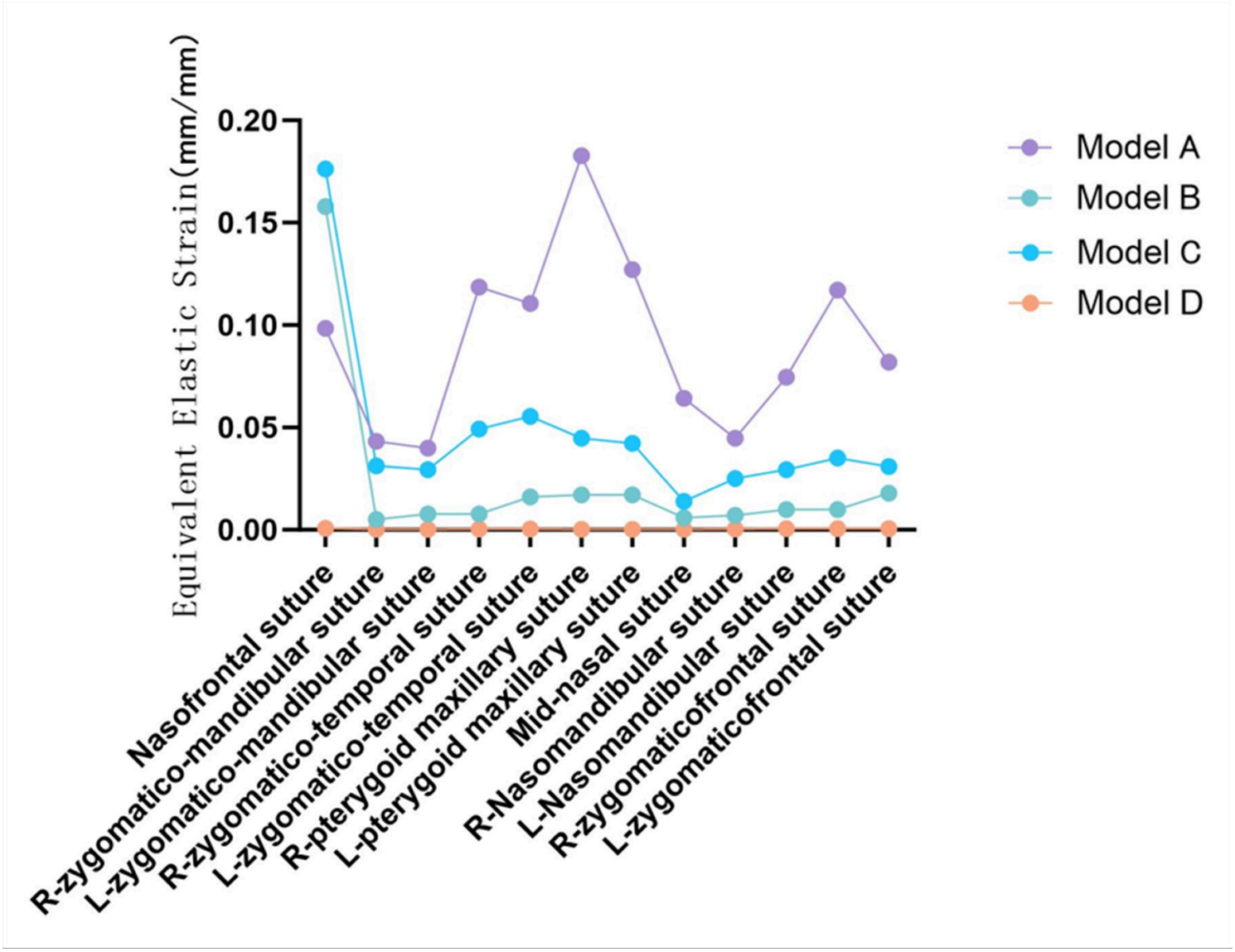


Figure 4

shows the displacement trend and stress distribution of the midpalatal suture following arch expansion, presented in the form of a cloud diagram.

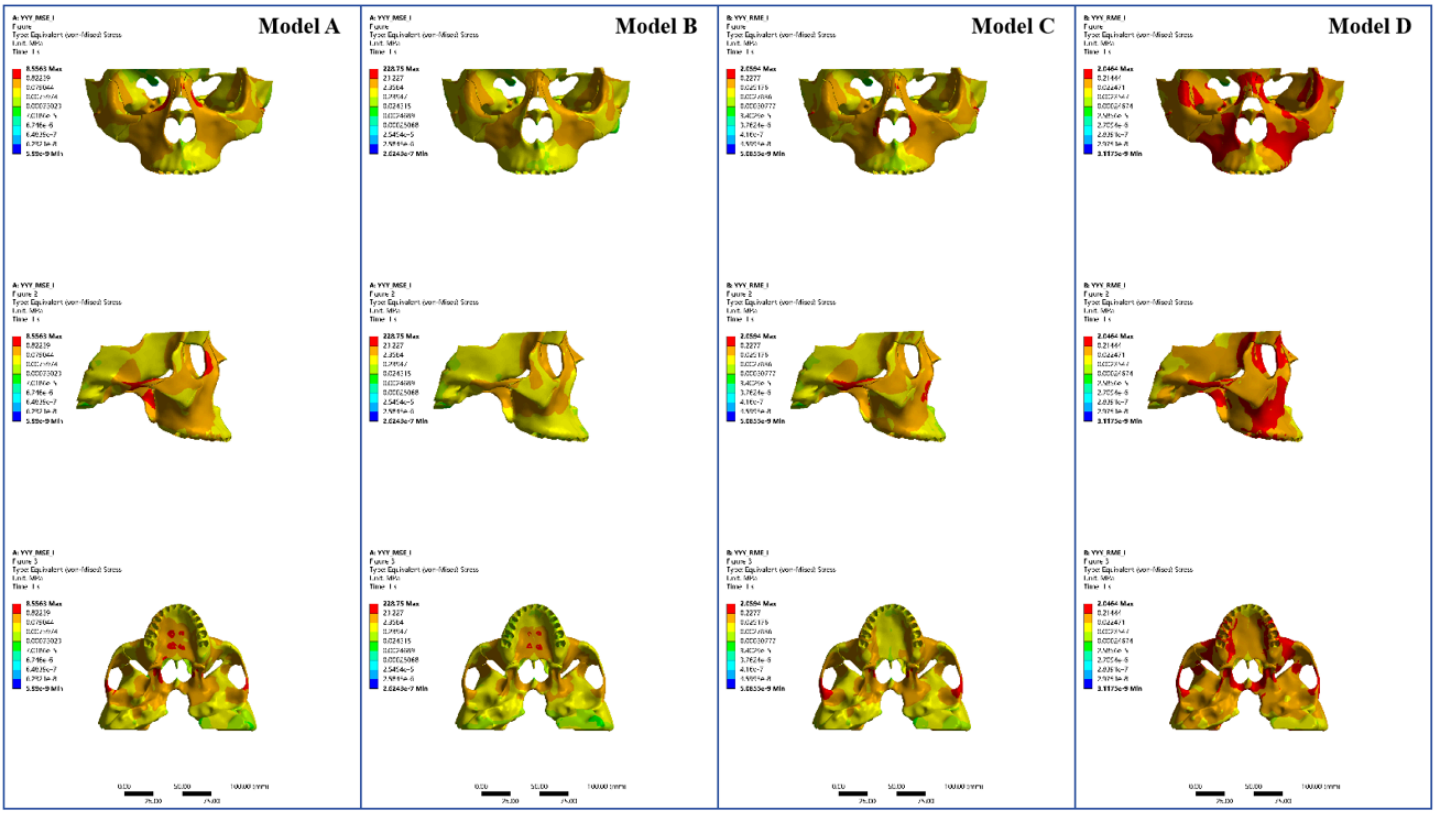


Figure 5

show the stress clouds and displacement trends, respectively, of the cranial maxilla.

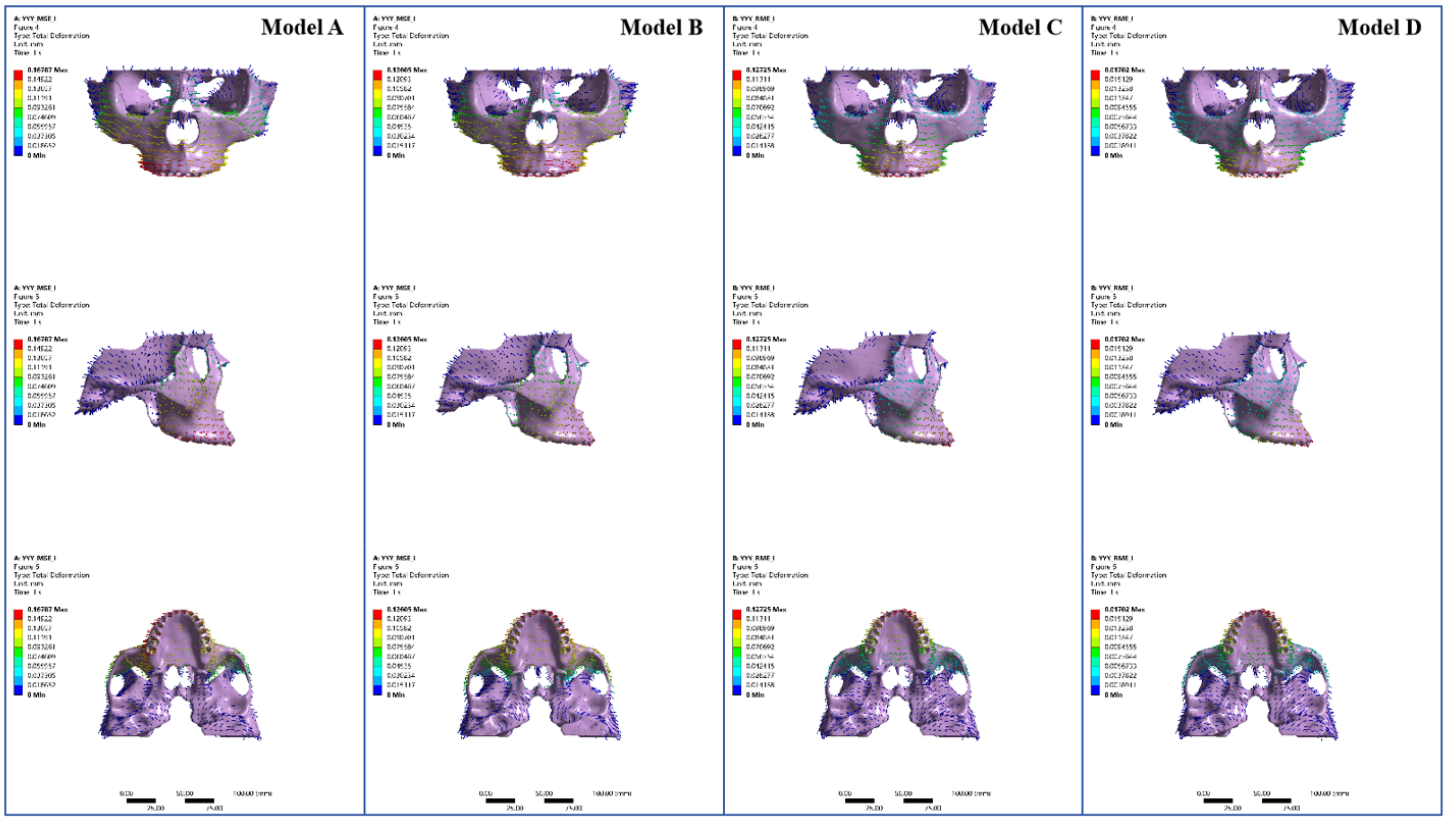


Figure 6

show the stress clouds and displacement trends, respectively, of the cranial maxilla.

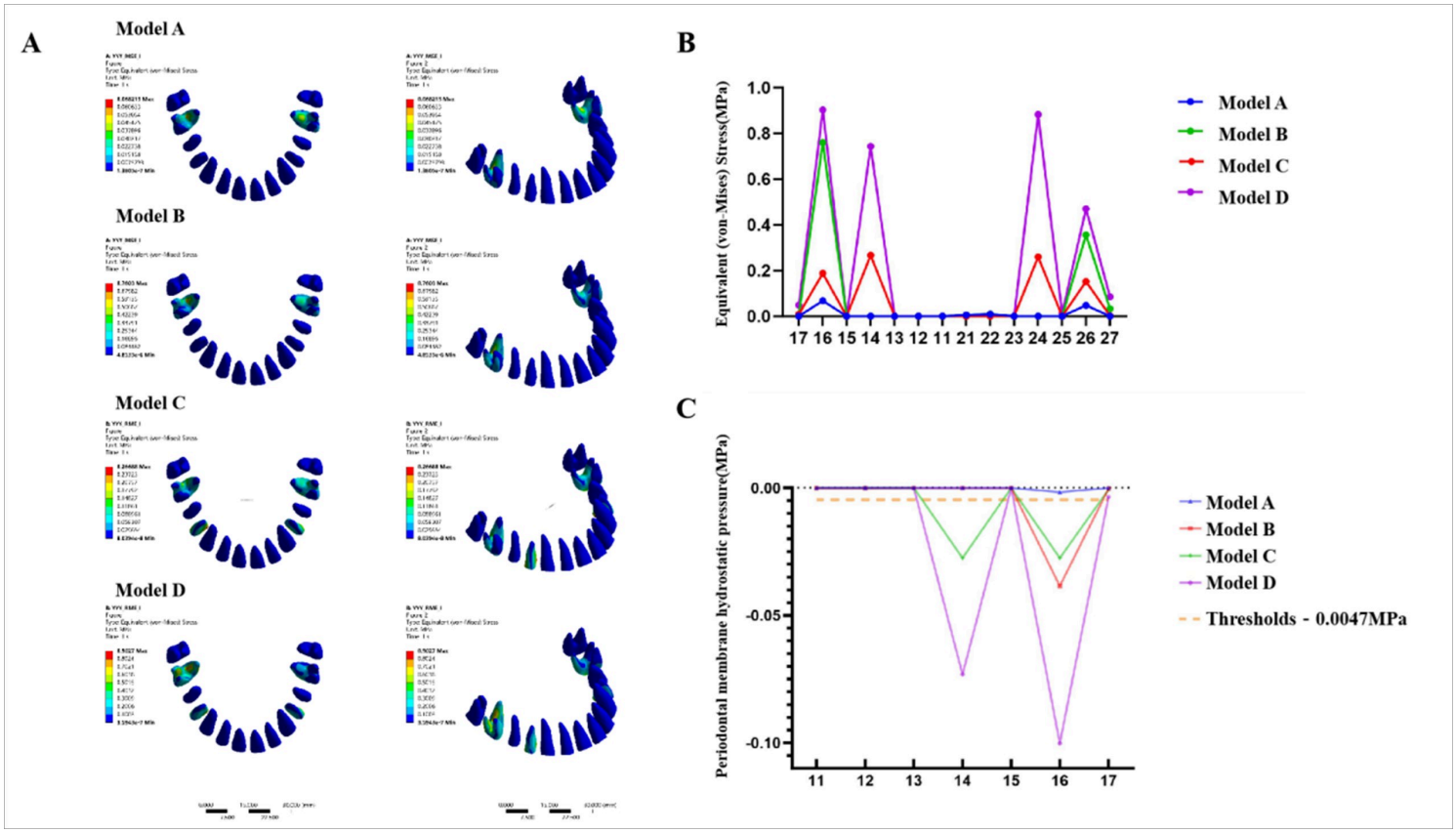


Figure 7

A shows the distribution of the equivalent stresses on the tooth roots in a cloud view.B shows the distribution of equivalent forces in the context of tooth root structures.and C shows that the value of hydrostatic stress in the periodontium may serve as an indicator of root resorption. A previous study revealed a threshold value of capillary pressure in the periodontal ligament (PDL) of 0.0047 MPa.

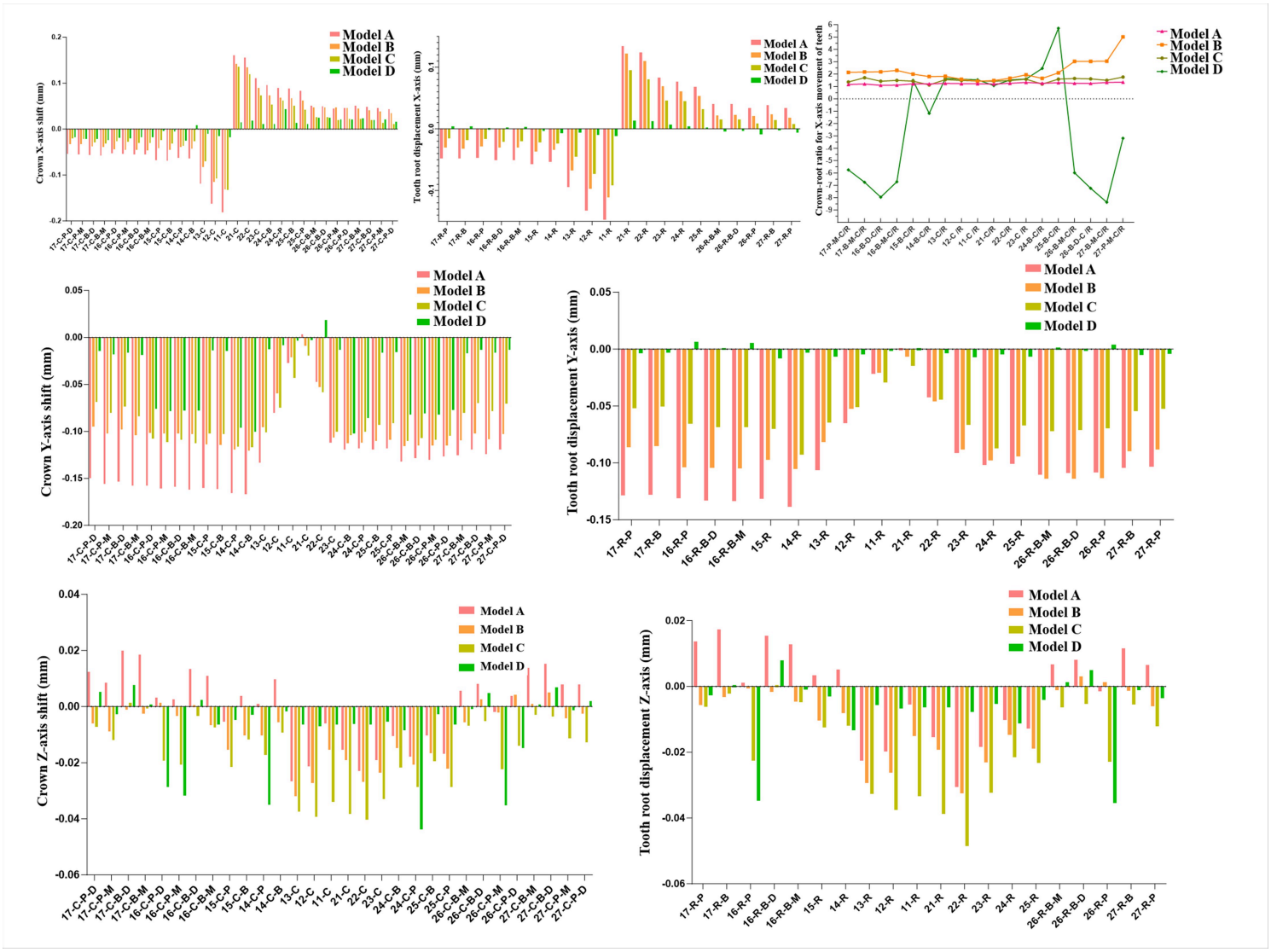


Figure 8

illustrates the three-dimensional directional displacement of tooth marker points.